JGR Space Physics

RESEARCH ARTICLE
10.1029/2018JA026415

The Effect of Ozone Shadowing on the *D* Region Ionosphere During Sunrise

Edith L. Macotela[1], Mark A. Clilverd[2], Jyrki Manninen[1], Neil R. Thomson[3], David A. Newnham[2], and Tero Raita[1]

[1]Sodankylä Geophysical Observatory, University of Oulu, Sodankylä, Finland, [2]Space Weather and Atmosphere, British Antarctic Survey (UKRI-NERC), Cambridge, UK, [3]Department of Physics, University of Otago, Dunedin, New Zealand

Key Points:
- Subionospheric radio wave measurements show a sunrise transition during which a phase perturbation is often observed
- Sunrise phase perturbation amplitude is better correlated with stratospheric ozone number density than with atmospheric temperature
- Sunrise phase perturbation is principally generated by stratospheric ozone shadowing of the *D* region ionosphere

Correspondence to:
E. L. Macotela,
edith.macotelacruz@oulu.fi

Citation:
Macotela, E. L., Clilverd, M. A., Manninen, J., Thomson, N. R., Newnham, D. A., & Raita, T. (2019). The effect of ozone shadowing on the *D* region ionosphere during sunrise. *Journal of Geophysical Research: Space Physics*, *124*, 3729–3742. https://doi.org/10.1029/2018JA026415

Received 18 DEC 2018
Accepted 15 APR 2019
Accepted article online 25 APR 2019
Published online 23 MAY 2019

Abstract Diurnal very low frequency subionospheric radio wave phase measurements show a night-to-day transition pattern. During this sunrise transition a phase perturbation, which consist of a phase overshoot followed by a small phase recovery to normal daytime values, is often observed. The variability of the size of this sunrise phase perturbation and its maximum and end times were monitored to identify the associated physical causes. Very low frequency signal from the 22.1-kHz UK transmitter (call sign GVT) recorded at Sodankylä, Finland, from 20 April 2010 to 31 December 2016 were used. The timing at the maximum of the phase perturbation period has an annual pattern that is well described by the seasonal variation of the sunrise time 28 km above the transmitter. Variations in ozone number density at 38–42-km altitudes are better correlated ($R = 0.7$) with the sunrise phase perturbation variability than at any other altitudes below ~80 km, and exhibit higher correlation values than for atmospheric temperature. Our results show that the main characteristics of the observed very low frequency sunrise phase perturbation arise from shadowing of short-wavelength solar UV flux from the *D* region ionosphere due to stratospheric ozone absorption.

1. Introduction

Very low frequency (VLF; 3–30 kHz) radio signals propagate inside the Earth-ionosphere waveguide and can be used to monitor the electrical conductivity of the waveguide's boundaries (Wait & Spies, 1964). For a VLF signal from a given man-made transmitter recorded at a specific location the most prominent changes in the waveguide are due to the passage of the sunrise and sunset terminators (Bracewell & Straker, 1949). Depending on the orientation of the terminator to the direction of the VLF path the transitions can last between minutes and hours (Lynn, 2010). At some receiver locations, the sunrise transition is observed in the VLF phase measurements as a large phase overshoot followed by a phase recovery prior to normal daytime values. This phenomenon will be known throughout this work as a sunrise phase perturbation (SPP). Previously, SPP has been described as a sunrise dip (Bracewell & Bain, 1952), or a phase instability observed after the end of sunrise (Reder & Westerlund, 1970). However, for clarity we will adopt the use of "sunrise phase perturbation", and will estimate its properties using the closest normal daytime values exhibited in the VLF phase data.

Previous studies have used the SPP size, which is the phase difference between its maximum and end values, to characterize them (Abdu et al., 1973; Bertoni et al., 2013; Comarmond, 1977; Hargreaves, 1962; Kuntz et al., 1991; Reder & Westerlund, 1970). Those studies reported that (i) the SPP size depends on the time of year; that is, it depends on the season, with more day-to-day variability during wintertime than during summertime (e.g., Hargreaves, 1962); (ii) SPP is best observed and also has higher values when the morning terminator crosses a VLF signal path at very small angles (e.g., Reder & Westerlund, 1970); (iii) there is evidence of a latitudinal dependence of SPP, which increases in size with increasing latitude (Abdu et al., 1973), and also a dependence with the frequency, which increases in size when the VLF transmitting frequency increases (Comarmond, 1977); (iv) SPP can last less than 1 hr (Kuntz et al., 1991); (v) SPP depends on the epoch of the 11-year solar cycle, being a minimum at solar maximum (Kuntz et al., 1991); and (vi) the solar illumination conditions, that is, solar zenith angle values, and the geometrical configuration of a VLF path relative to the sunrise terminator partly explain the SPP size variation observed during summertime (Bertoni et al., 2013). Bertoni et al. (2013) also reported a similar seasonal behavior between the SPP size and mesospheric temperature variations; however, no one-to-one correspondence was found.

Bracewell and Bain (1952) and Hargreaves (1962) suggested that the phase perturbation observed during sunrise was evidence of an ionospheric layer below the *D* region. During sunrise solar radiation initially impinges the upper atmosphere producing rapid photodetachment. Then, the solar radiation gradually illuminates lower altitudes as the sunrise progresses; that is, as the solar zenith angle (SZA) decreases. Therefore, during sunrise a sharp discontinuity in the electron profile, at the altitude illuminated by solar rays, is created (Moler, 1960). This electron profile discontinuity was called the *C* layer by Krasnushkin (1962), to differentiate it from the *D* region that is created by photoionization (Nicolet & Aikin, 1960). Rocket measurements showed an ionospheric layer below the *D* region formed near sunrise between solar zenith angles of ~94° and ~85° (Mechtly et al., 1967; Mechtly & Smith, 1968; Sechrist, 1968). In addition, Turco and Sechrist (1972) proposed that at sunrise the photodissociation of molecular oxygen would lead to associative detachment between O_2^- and O resulting in an increase in the number of free electrons. According to Ratcliffe (1972), this associative detachment could explain the observation of abrupt changes in the VLF measurements during sunrise.

The importance of studying the SPP is because it could provide information about the amount of negative ions present in the lower ionosphere. Clearly, more understanding of the SPP properties is needed in order to fully understand the causative effect. Therefore, it is essential to undertake further analysis of the SPP behavior by taking into account seasonal variations in its magnitude and occurrence characteristics. Additionally, many previous studies analyzed the SPP using low- to middle-latitude VLF propagation paths. Therefore, there is a lack of knowledge regarding the SPP variability effect at high-latitude regions. Furthermore, none of these studies used the SPP maximum or end time, which detailed study can provide new information regarding the characteristics of this phenomenon.

The aim of the present study is to examine the SPP properties, on a quasi-polar subionospheric VLF propagation path to identify the physical causes of SPP variations. With that in mind, the size of SPPs and their maximum and final times were analyzed. By determining the maximum and final times we are able to investigate their temporal variability. By calculating the size of SPP, we are able to examine its association with atmospheric parameters such as mesospheric temperature and stratospheric ozone number density. In section 2, the data sets used in this work are presented. The results obtained and their interpretation are presented and discussed in sections 3 and 4, respectively. Finally, section 5 summarizes the conclusions of this study.

2. Observational Data

To undertake this study, VLF phase measurements recorded in northern Finland were used as well as stratospheric and atmospheric temperature, and ozone volume mixing ratio (vmr) data from a near-polar orbiting satellite. The use of these data sets brings the advantage of comparing the results of the present study with those of Bertoni et al. (2013) who used similar data sets. This section contains a description of the experimental setup and an explanation of the methodology applied to characterize the SPP observed during sunrise, along with the atmospheric temperature and ozone vertical profile.

2.1. Ground-Based VLF Measurements

In this study, the narrow band subionospheric VLF data from the 22.1-kHz transmitter (call sign GVT; 54.7°N, 2.9°W), located in UK, and recorded at Sodankylä, Finland (SOD; 67.4°N, 26.7°E) were used. The Sodankylä receiver is part of the Antarctic-Arctic Radiation-belt (Dynamic) Deposition–VLF Atmospheric Research Konsortium network (Clilverd et al., 2009) which provides continuous long-range observations of the lower ionosphere in the polar regions. The receiver is composed of two orthogonally orientated loop antennas, and the recording system uses the UltraMSK software, which measures both the phase and amplitude of Minimum Shift Keying (MSK) modulated narrowband VLF radio signals (Clilverd et al., 2009). The spatial configuration of the transmitter (GVT) and receiver (SOD) are shown in Figure 1. In this figure, the great circle propagation path between the two radio stations is shown as a blue curve. The black rectangle represents the area near the transmitter from which atmospheric data from the Aura satellite are analyzed and compared with the VLF phase data. The reason for this choice lies in using the atmospheric data that best represent the conditions at the transmitter because, as will be shown in the result section, most of the times at the maximum of SPP matches with the sunrise time above the transmitter which, being at the western end of the path, represents the last part of the path

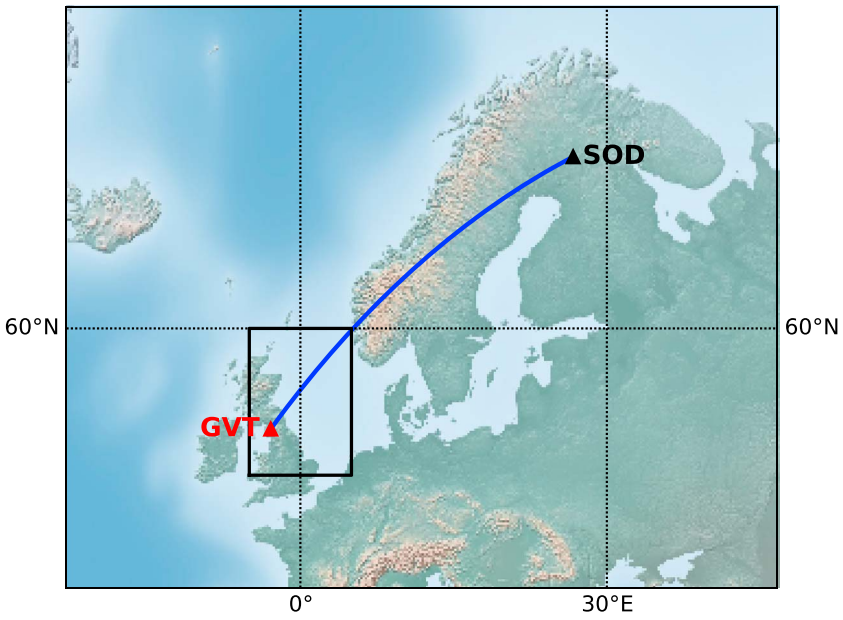

Figure 1. Map showing the location of the VLF transmitter GVT and receiver SOD, and the propagation path between these two stations (blue curve). The black rectangle represents the area where atmospheric data from the Aura satellite are analyzed (see section 3.2).

to undergo the sunrise transitions. From the map it is observed that more than half of the propagation path is at latitudes above 60°N.

Phase data from the GVT transmitter were recorded from the east-west loop aerial in Sodankylä from 20 April 2010 until 31 December 2016. A 24-hr temporal evolution of the VLF phase signal measured during 17 August 2010 is shown in Figure 2. The phase time profile illustrates deviations due to sunrise and sunset transitions over the VLF propagation path observed during the periods 00:00–05:00 UT and 18:00–22:00 UT, respectively.

During the sunrise transition (Figure 2: 00:00–05:00 UT) an elevated peak in the VLF phase, with respect to the daytime values (Figure 2: 05:00–18:00 UT), is observed. In this study, we concentrate on the sunrise phase perturbation part of the signal, that is, from the peak phase value to the start of daytime phase values. The amplitude of SPP (A_{sp}) is calculated as the difference between the maximum of the sunrise phase advance (ϕ_A) and the first minimum afterward ϕ_B. A representation of these two values is shown in Figure 2. Then, A_{sp} can be written as

$$A_{sp} = \phi_A - \phi_B \tag{1}$$

When calculating ϕ_A and ϕ_B the times associated with those values were also computed, that is, the times at which SPP is maximum (t_{spA}) and ends (t_{spB}). Using these two values, the duration (d) of SPP was computed:

$$d = t_{spB} - t_{spA} \tag{2}$$

2.2. Aura Satellite Data

The Earth Observing System Microwave Limb Sounder (MLS) onboard the Aura spacecraft measures thermal emission from the Earth's atmosphere (Waters et al., 2006). Aura coverage is from 80°N to 82°S, with ~13 orbits per day, limb scanning from close to the ground up to approximately 100 km. The MLS instrument provides daily global measurements of vertical profiles of temperature and chemical constituents, such as ozone (Waters et al., 2006). The MLS v4.2x level 2 temperature and ozone vmr data, which are used in this study, have been screened using the quality control criteria of Livesey et al. (2017), that is, using only the recommended vertical pressure range for scientific use of 261–0.001 hPa for the temperature data, and 261–0.01 hPa for the ozone data. We have also used data with the recommended quality thresholds,

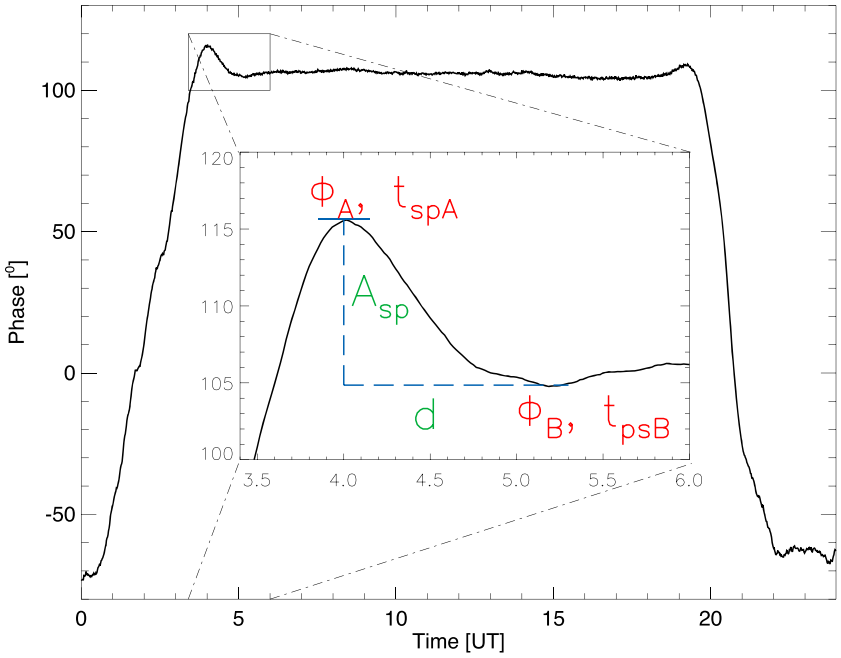

Figure 2. Diurnal phase evolution of the 22.1-kHz transmitted signal from GVT observed at Sodankylä on 17 August 2010. The time profile of the phase illustrates deviations due to sunrise and sunset transitions over the VLF propagation path during the periods 00:00–05:00 UT and 18:00–22:00 UT, respectively. The phase value (ϕ_A, ϕ_B) at the maximum and end times of SPP (t_{spA}, t_{spB}) as well as the size of SPP (A_{sp}) and its duration (d) are indicated.

convergence thresholds, status flags, and estimated precisions. We utilize the MLS measurements for the period from 1 January 2010 to 31 December 2016, and for the region within the black rectangle in Figure 1. The area is located between 52°N and 60°N, and between 5°W and 5°E.

An overview of the atmospheric temperature data set used in this study is shown in Figure 3, where the atmospheric regions up to the mesosphere can be clearly differentiated. At the same time, a seasonal dependence, that is, high variability in temperature during wintertime and low variability during summertime, is observed. In this figure, white regions indicate missing data. The horizontal lines indicate three different altitude ranges of temperature variability used in this study, namely, 36–40, 64–68, and 83–87 km. The temperature variations in these three atmospheric layers are analyzed in order to look for connections between the characteristics of SPP and temperature variations in the stratosphere, at altitudes corresponding to a reflecting *C* layer (Mechtly et al., 1967), and in the mesosphere, respectively.

The ozone vmr data were converted to ozone number densities by applying the ideal gas equation, in order to determine the amount of ozone that could potentially influence solar UV radiation reaching the *D* region. Figure 4 illustrates an overview of the ozone number densities, where the white regions indicate missing data. In this figure, ozone shows seasonal variability, that is, high variability during northern hemisphere wintertime and low variability during summertime, particularly at ~40 km. Horizontal lines indicate three altitude ranges, namely, 19–23, 38–42, and 50–54 km. We examine ozone number density variability in these three layers to look for connections with A_{sp} variability. These altitude ranges differ from those chosen for the atmospheric temperature analysis because the aim is to identify the altitudes where maximum ozone shadowing of solar UV radiation occurs. These heights could be at the maximum of ozone density or where the seasonal gradient change is important.

3. Results

In this section, the observed variability of both A_{sp} (section 3.1) and t_{spA} (section 3.2) are characterized. At the same time, the relationships between A_{sp} and atmospheric temperature, and between A_{sp} and ozone, are examined (sections 3.3 and 3.4).

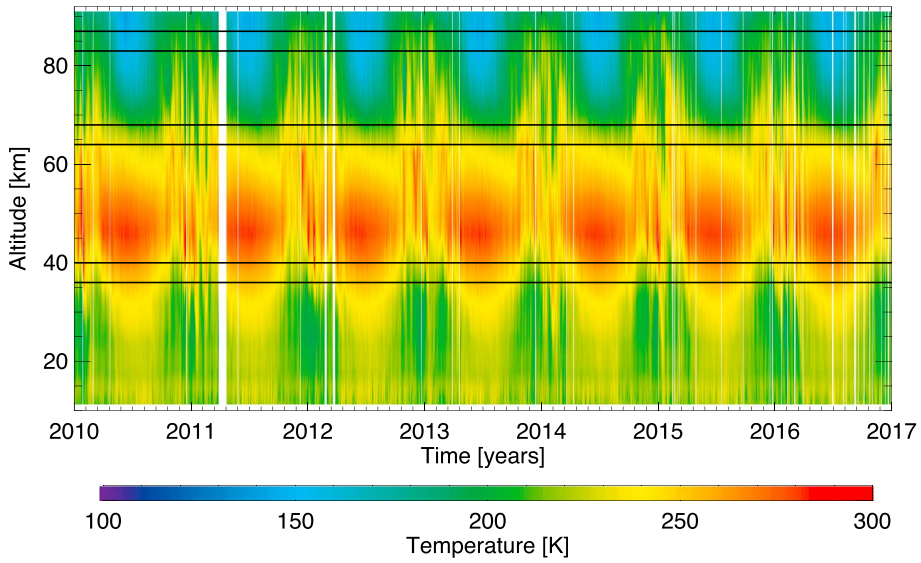

Figure 3. Vertical overview of daily MLS atmospheric temperature since 2010 until the end of 2016, for the latitudes between 52°N and 60°N, and longitudes between 5°W and 5°E. The horizontal lines represent the boundaries of three different altitude ranges of interest, that is, 36–40, 64–68, and 83–87 km.

3.1. A_{sp} Variability

Figure 5 shows the variabilities of the SPP size, A_{sp}, atmospheric temperature, and ozone number density as a function of day of year. Figure 5a displays the daily A_{sp} values, color-coded according to the year of measurement, from 20 April 2010 until the end of 2016. The black curve in Figure 5a is the average A_{sp} time profile for years 2010–2016 smoothed using a five-day time window length. This curve shows that there is an annual variation of A_{sp} with lower average values during the northern hemisphere summertime (days 130–230) and higher values during the wintertime (days 1–100 and 280–365). A_{sp} variability during the summer is also less than that observed during the rest of the year. Both observations are consistent with previous findings, which have been summarized in section 1.

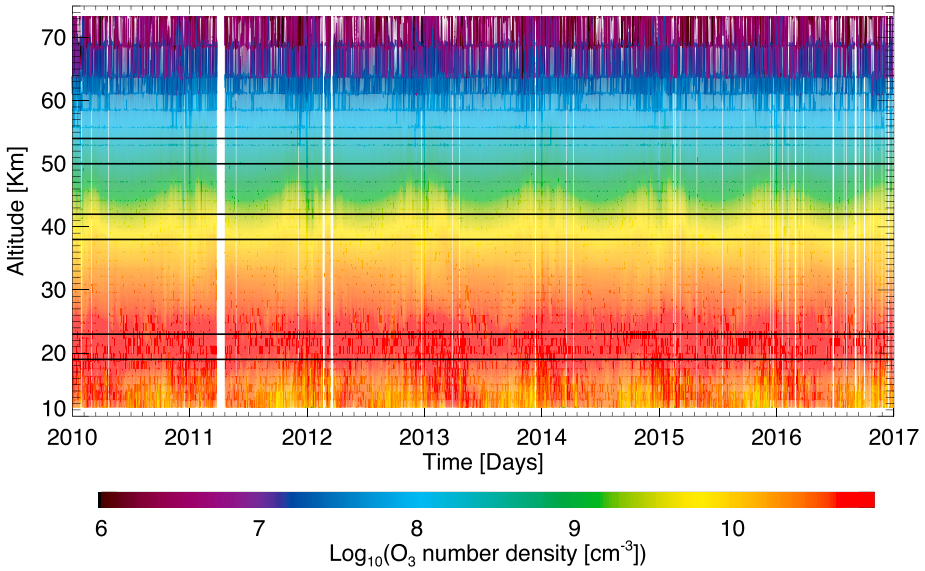

Figure 4. Time series of atmospheric ozone number density profiles from 2010 until the end of 2016, for the latitudes between 52°N and 60°N, and longitudes between 5°W and 5°E. The horizontal lines represent the boundaries of three different altitude ranges, that is, 19–23, 38–42, and 50–54 km.

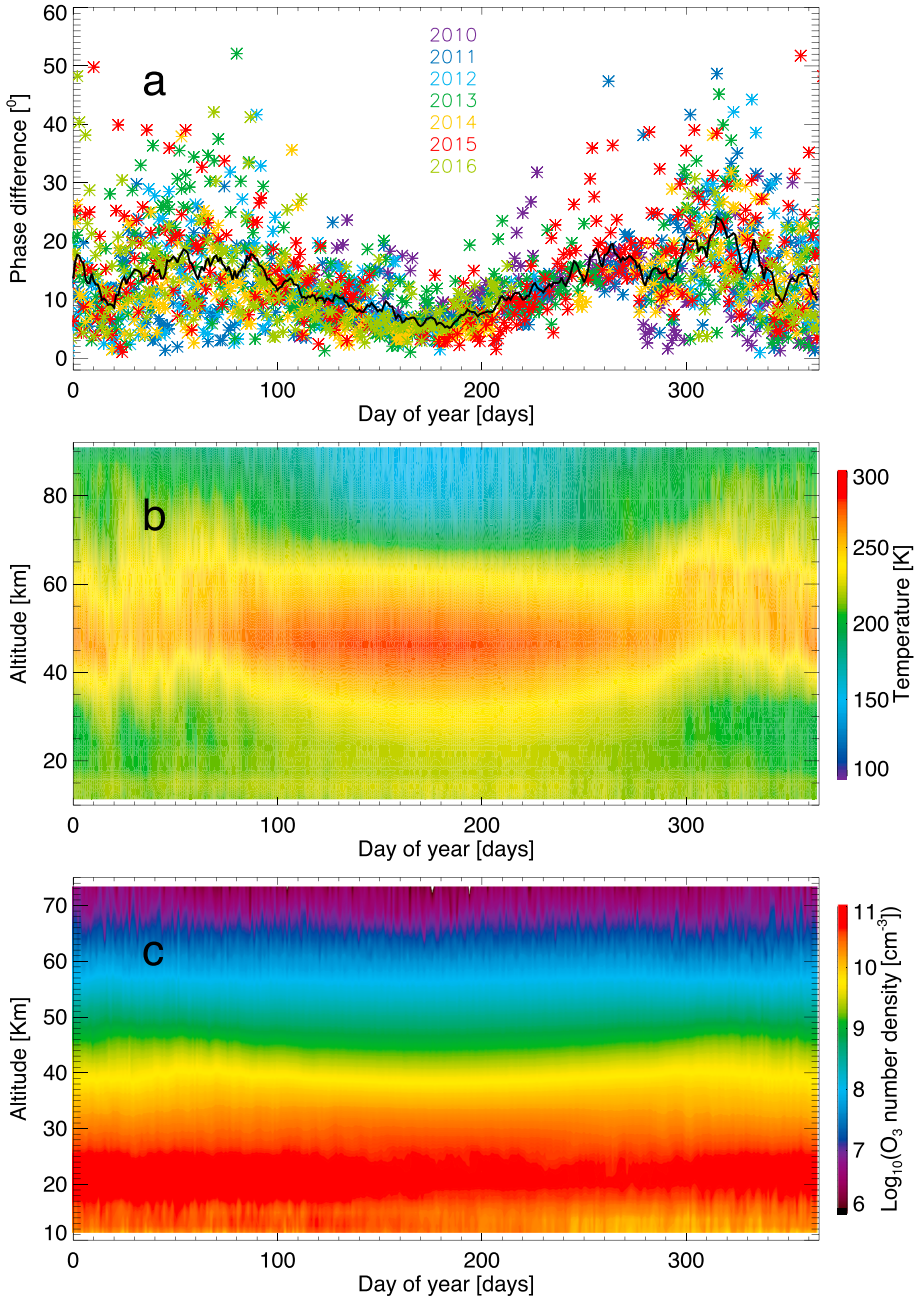

Figure 5. (a) Variability of A_{sp}, (b) atmospheric temperature height profile, and (c) ozone electron density height profile as a function of day of year. The black curve in (a) is the five-day smooth of A_{sp} averages daily values from 2010 to 2016.

Figure 5b shows the average atmospheric temperature height profile as a function of day of year, where the white regions indicate missing data. The average values were computed using data from the beginning of 2010 until the end of 2016. Figure 5c shows the corresponding variability in the ozone number density. As is observed in Figures 3 and 4, the temperature and ozone data in Figures 5b and 5c show clearly different atmospheric variabilities up to the mesosphere (~50 km). However, a seasonal dependence, that is, high variability during wintertime and low variability during summertime, is more evident in atmospheric temperature than in ozone number density, because the high variability observed in wintertime ozone in Figure 4 is smoothed out in Figure 5c.

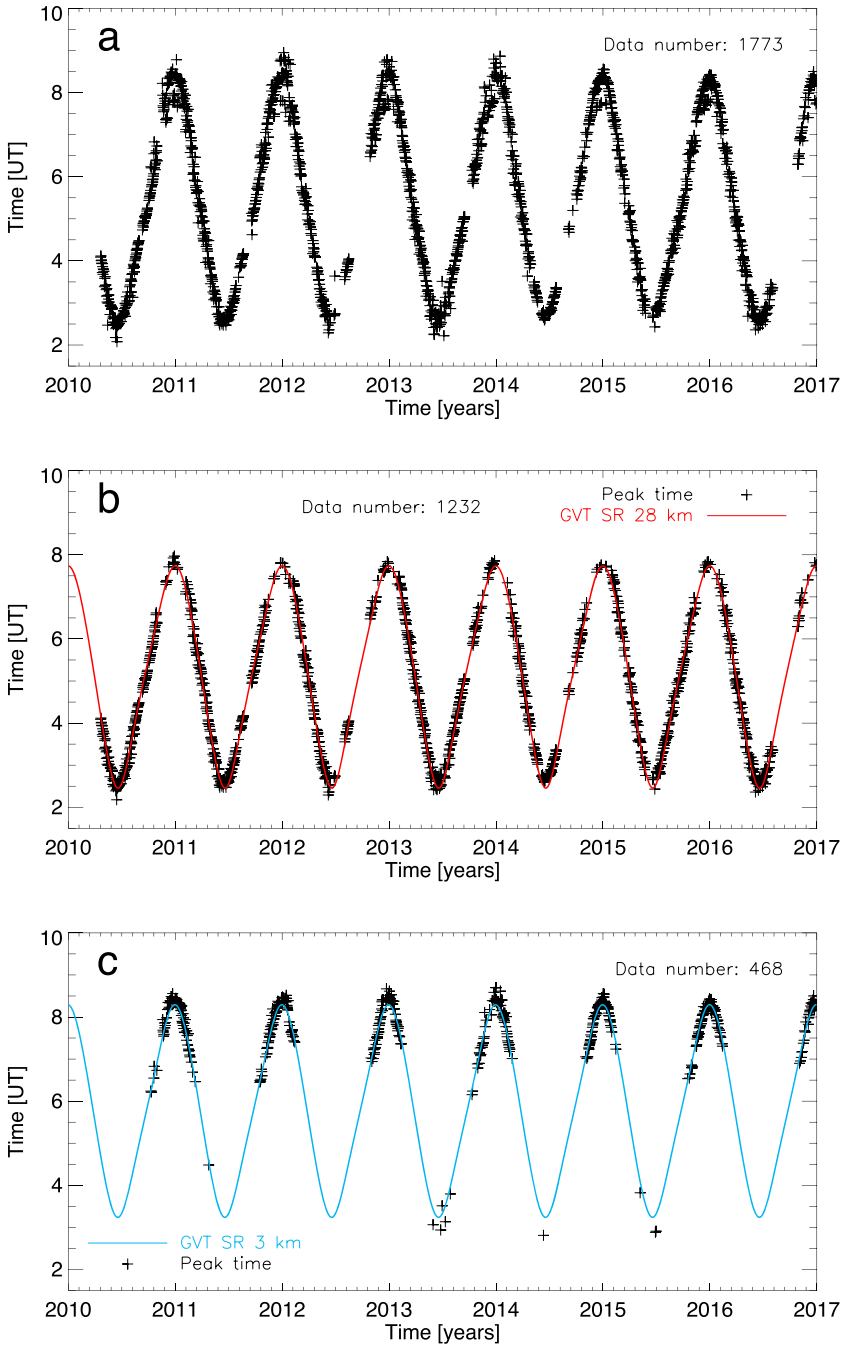

Figure 6. (a) Temporal evolution of the time at the maximum sunrise phase perturbation of the 22.1-kHz transmission from England (GVT), UK, received at Sodankylä (SOD), Finland. (b and c) Selected data (cross symbol) for sunrise times at 28 km (red curve) and at 3 km (cyan curve) above the VLF transmitter, respectively.

3.2. t_{spA} Variability

Figure 6 shows, as black symbols, the temporal variation of the time at the maximum of SPP (t_{spA}) from April 2010 until the end of 2016. Figure 6a shows all the data set of t_{spA}, where the gaps correspond to periods of transmitter or receiver downtime, that is, when no observations were collected. Notably, this figure demonstrates a well-defined seasonal variation that resembles the change in the occurrence times of SZA over the year. However, because the analysis is for the sunrise time period, we assumed that t_{spA} is most likely to be

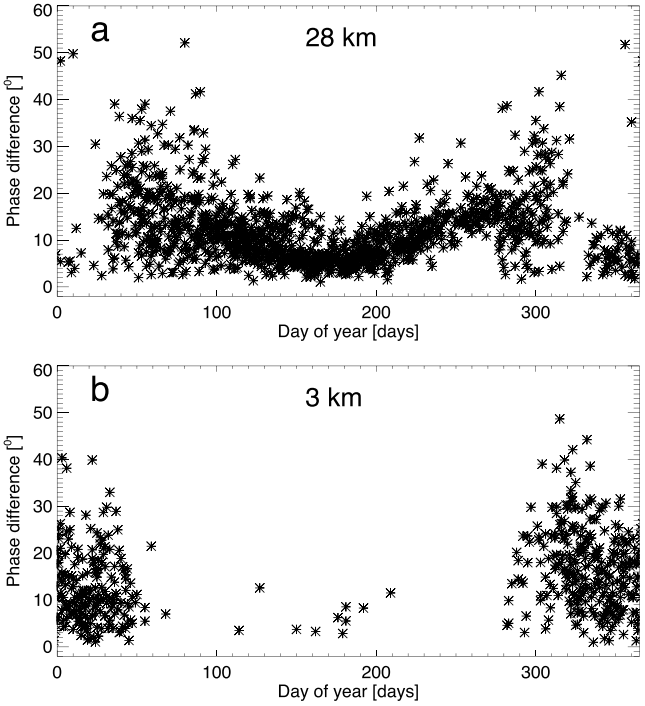

Figure 7. Annual variation of A_{sp} for 2010 to 2016 differentiated according to their association with a sunrise time at (a) 28 km and (b) 3 km, respectively, above the VLF transmitter.

associated with sunrise time at a certain location along the propagation path between the transmitter and the receiver. To determine this location, the VLF path was divided into 20 parts. Then, the sunrise time was computed at every point and at 1-km intervals from ground level to 90-km altitude. In the computation, atmospheric refraction near the horizon was not considered in order to match the times with the ones given by the *Astronomical Almanac*.

Figure 6a indicates two timings grouped at ~08:00 UT during each wintertime. In order to find the best match between t_{spA} and the computed sunrise times, the minimum difference of these two time sets, outside of the winter season, was estimated. This minimum difference was found for sunrise 28 km above the transmitter location, and was therefore extended to all times of year. Figure 6b shows the t_{spA} data that were identified from those best matches, which make up 69% of the timings. The same minimum difference technique was then applied to the remaining data, producing the result shown in Figure 6c. In this case, the best match is found for sunrise 3 km above the transmitter location. The red and blue curves in Figure 6 represent the sunrise time at 28 and 3 km above the transmitter, respectively. Because the sunrise times at the transmitter best represent the t_{spA} variation, we select atmospheric satellite data sets close to the transmitter location to undertake comparisons with the VLF data. For the comparison, data from the same days were used. In addition, we verified that for altitudes above 4 km, the transmitter end, rather than the receiver end, is the last part of the VLF path to undergo the sunrise transition. We found no correspondence between t_{spA} and the times for SZA variation for 80°–96°, in the 20 divided sections of the VLF path, confirming that t_{spA} variability is related to the sunrise time variability.

These results strongly suggest that the amplitude of SPP in the course of the sunrise transition could involve processes occurring at stratospheric altitudes, that is, ~28 km. Such a mechanism could involve stratospheric screening of solar radiation at high SZA from reaching the ionospheric *D* region. The results also suggest that the source of this screening is more variable throughout the winter season. Because solar UV radiation is absorbed by stratospheric ozone, we postulate that the shadowing of solar radiation by ozone controls the amplitude of the sunrise phase perturbation observed during the sunrise transition as is shown in Figure 4 of Sechrist (1968). On the other hand, Figures 6b and 6c illustrate that during wintertime the altitude where ozone produces greatest shadowing varies. Thus, the altitude variability of ozone number density during wintertime may explain the day-to-day variability of A_{sp}.

In order to test the above hypothesis, we separate the A_{sp} values according to the times associated with sunrise at 3 and 28 km. Figure 7 shows the superimposed annual variation of A_{sp}, as a function of day of year, from April 2010 until December 2016. The upper panel refers to the A_{sp} data whose t_{spA} best matches with sunrise times at 28 km, and the lower panel refers to the data whose t_{spA} best agrees with sunrise times at 3 km. This figure demonstrates that the majority of A_{sp} variability in wintertime is associated with sunrise time 3-km altitude above the transmitter.

3.3. t_{spB} Variability and the Sunrise Phase Perturbation Duration

Additionally, the time at which SPP ends (t_{spB}) was also analyzed. From t_{spB} onward the expected daytime SZA dependence of the *D* region influence on subionospheric propagation is observed (Thomson et al., 2017). This is consistent with the idea that no further stratospheric screening occurs after SPI, as solar illumination of the *D* region is then unrestricted; that is, stratospheric ozone shadowing of UV radiation is not occurring. Similar to the t_{spA} observations shown in section 3.2, t_{spB} observations demonstrate a well-defined temporal variation, observed especially during summertime, which resembles changes in SZA over the year. Unexpectedly, t_{spB} times during the winter period are not well defined; in other words, there are not two groups as was the case for t_{spA}.

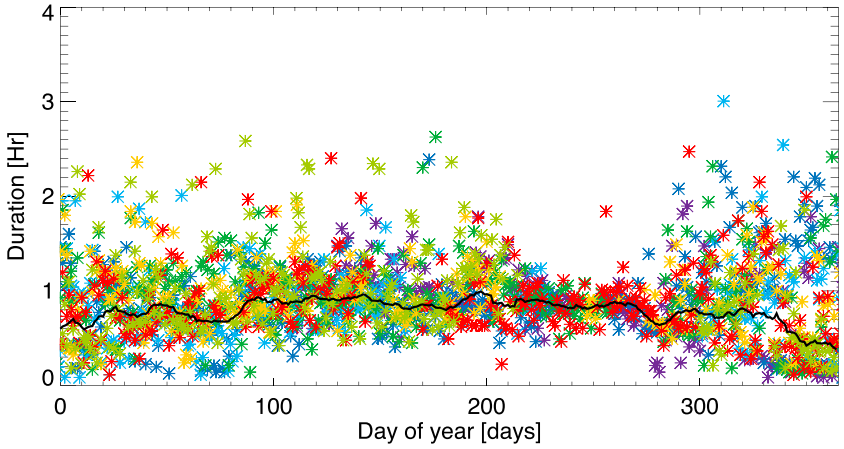

Figure 8. Annual variation of the daily duration of SPP, as a function of day of year, for 2010 to 2016. The black curve is a 10-day moving average of the daily mean *d* values.

To determine location of the sunrise times and/or SZA that best match t_{spB} we proceed as explained in section 3.2. We found that SZA in the range 88°–90° in the vicinity of the transmitter match the observations. Undertaking calculations for this location, a SZA of 90° provides the best match with the observed VLF variability, particularly during summertime.

Figure 8 shows the temporal variability of the daily SPP duration (*d*) from 2010 until 2016. In this figure, the black curve shows the time profile of the average *d* values, computed for values <1.3-hr duration, smoothed using a 10-day moving average. The smoothed curve suggests that the SPP duration is ~20% shorter during winter than during summer. However, the average SPP duration is 54 ± 10 min (1 standard deviation; i.e., ±1σ), and the magnitude of the seasonal variation is similar to this uncertainty range.

3.4. A_{sp} and the Atmospheric Temperature Relationship

Figure 9 shows the temporal variability of A_{sp} (black curve) compared with atmospheric temperature (orange curve), using the days of the time matchings explained in section 3.2, averaged over three different altitude ranges (36–40, 64–68, and 83–87 km). Both time series were averaged using a time window length of 10 days. Gaps in the VLF data correspond to transmitter or receiver downtime, when no observations were collected. In this figure, the correlation coefficients (*R*) between the A_{sp} and temperature time series are given in the legend boxes. Note that in Figure 9c the 36–40-km temperatures are plotted on an inverted scale.

The most dominant pattern in Figure 9 is the annual oscillation that can be seen in A_{sp} and temperature in all three altitude ranges. Good correlation is found between A_{sp} and temperatures at 83–87 km, in the upper mesosphere. However, the correlation with 83–87-km temperatures is dominated by the strong annual variation. On the other hand, the 36–40-km temperatures show not only a similar annual variation to A_{sp} but also similar double-peaked behavior in winter. As a result, the best correlation ($R = -0.66$) is between A_{sp} and the MLS measured temperatures at 36–40 km. Thus, an increase of A_{sp} usually coincides with decreased temperatures in the stratosphere at 36–40 km, and this behavior can be seen on seasonal and annual time scales.

3.5. A_{sp} and the Atmospheric Ozone Relationship

The suggestion that the ozone layer produces screening effects on solar radiation during sunrise hours was first reported by Bracewell and Bain (1952). This screening effect is important in the creation of electron density profiles in the sunrise *D* region. Bracewell and Bain (1952), using VLF data, found that sunlight affects the *D* region ionosphere when the solar disk is depressed 8° below the horizon, that is, with solar radiation incident on the ionosphere from below. Moler (1960) modeled the electron density profiles and showed that the onset of photodetachment in the lower ionosphere starts when the solar rays become tangent to a surface 35 km above the Earth. He suggested that absorption by ozone at altitudes below 35 km causes a significant reduction of photodetachment energy. Hultqvist (1966) used data recorded by different radio techniques and

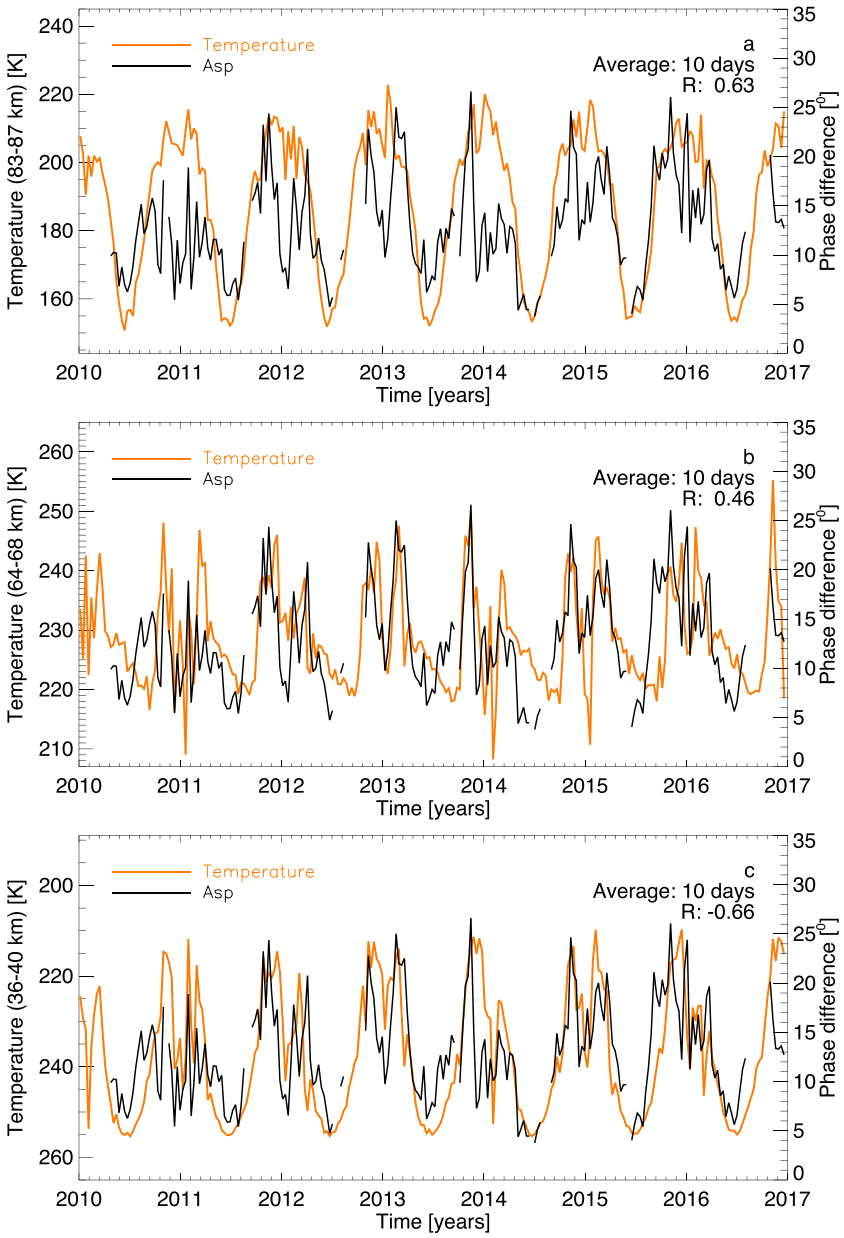

Figure 9. The 10-day averages of A_{sp} variability (black curve), using the days of the time matchings explained in section 3.2, contrasted with the atmospheric temperature (orange curve) at (a) 83–87 km, (b) 64–68 km, and (c) 36–40 km. R is the correlation coefficient.

observed that the electron density changes are more consistent with a lower ionosphere controlled by the shadow of the ozonosphere rather than by the solid Earth's shadow. Sechrist (1968) estimated the effective height above which photodetachment of electrons from negative ions occur using electron density profiles obtained by rocket measurements. This effective ozone screening height is in the range 25–55 km. However, no analysis of the ozone influence on the size of the VLF sunrise phase perturbation was previously done. Thus, an analysis of ozone variability and the variability of A_{sp} is required to determine its relationship.

Figure 10 is the same format as in Figure 9, but showing MLS atmospheric ozone number densities rather than temperatures. Similar to the temperature analysis, the most dominant pattern in Figure 10 is the annual oscillation that can be seen in all of the time series. The highest correlation ($R = 0.70$) is between A_{sp} and ozone number density at 38–42 km. This correlation corresponds to a p value of 1×10^{-7}, which means

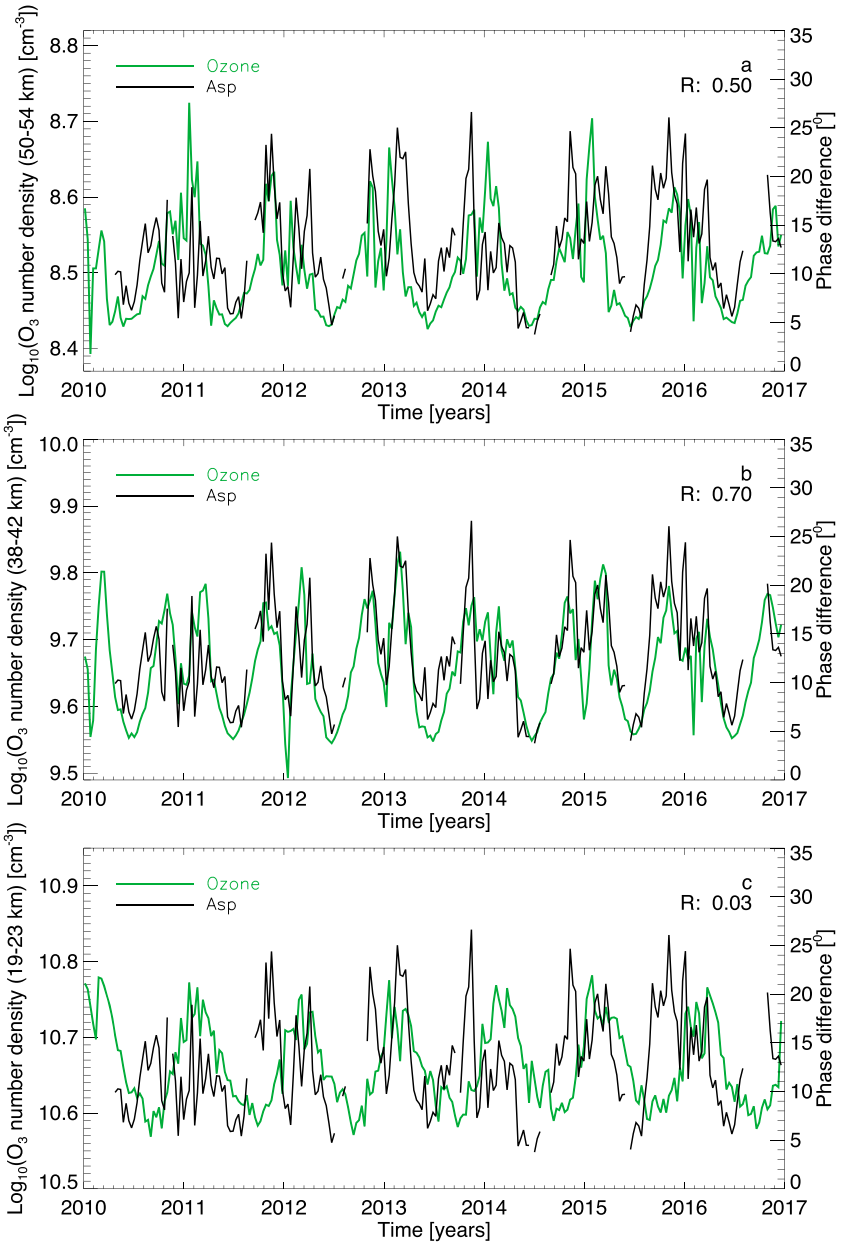

Figure 10. The 10-day averages of A_{sp} variability (black curve), using the days of the time matchings explained in section 3.2, contrasted with the atmospheric ozone number density (green curve) at (a) 50–54 km, (b) 38–42 km, and (c) 19–23 km. R is the correlation coefficient.

that the correlation is statistically significant at the 99.9% level. Outside of this altitude range the correlations are weaker, with poor agreement during wintertime. We note that ozone values at altitudes below ~80 km were also tested. The ozone data for the three altitude range shown in Figure 10 are representative of the overall results, with the 38–42-km altitude range showing the highest correlation. Thus, we find that an increase of A_{sp} usually coincides with increased ozone number density in the middle to upper stratosphere.

4. Discussion

The present study shows that the size of SPP is seasonally dependent, with smaller values observed during summertime and larger values during wintertime. Also, the day-to-day variability in the size of SPP is larger in winter than in summer. These results agree with previous studies (e.g., Bertoni et al., 2013). This suggests

that the size of SPP measured in quasi-polar regions has, in general, similar characteristics to those previously measured at low- and middle-latitude regions.

The analysis presented here highlights three key findings. First, the timing at the maximum of the SPP period has an annual pattern that is well described by the seasonal variation of sunrise times at an altitude of 28 km above the VLF transmitter. Second, atmospheric temperature variations in the 36–40-km altitude range are better correlated ($R = -0.66$) with the size of SPP than temperatures at other altitudes. Third, atmospheric ozone number density at altitudes 38–42 km are better correlated ($R = 0.70$) with the size of SPP than ozone number density at any other altitude, and the correlation with ozone is higher than for atmospheric temperature. These three findings are key to understanding the driving mechanism for SPP.

The marked relationship, between the 10-day average of the size of SPP with atmospheric temperature at 36–40 km, and ozone number density at 38–42 km, suggests that the region above the peak in stratospheric ozone number density, at ~25 km, is important in the shadowing effect. Ozone shadowing occurs through absorption of UV wavelengths by stratospheric ozone as solar illumination at high SZA first impinges on the *D* region ionosphere at 75–85-km altitudes. This effect typically begins when the Sun is just rising above the horizon—as seen from an altitude of ~80 km—when solar illumination shines through a high partial column of ozone number densities at 15–40 km. This produces a shadow on the *D* region ionosphere, filtering solar UV flux, which is absorbed by the ozone (Sechrist, 1968). Only when the sun has risen sufficiently high above the horizon to directly illuminate the *D* region, without attenuation by stratospheric ozone, does the generation of the *D* region electron number density profiles at 70–90 km become well ordered by SZA effects (McRae & Thomson, 2000).

Preliminary models of the ozone screening effect on the lower ionosphere were reported previously (e.g., Hultqvist, 1966; Moler, 1960; Ratcliffe, 1972; Schaal & Ananthakrishnan, 1970; Sechrist, 1968). Using three rocket launches made during presunrise conditions at the midlatitude launch site, Wallops Island, Sechrist (1968) was able to associate ozone shadowing with resultant steep gradients in *D* region electron number density profiles. The steep gradients were thought to be generated as a result of an absence of short-wavelength solar UV flux, which altered the photodetachment rates of electrons from negative ions. From the measured altitudes of the steep *D* region gradients, the minimum ray height for photodetachment could be calculated (Sechrist, 1968), and the effective ozone shadow height for detaching UV radiation was found to be ~50 ± 5 km. The multiyear analysis presented here indicates that the screening altitude (38–42 km) is typically 8–12 km lower than indicated by earlier rocket measurements.

Under conditions of low solar illumination, the ionospheric sensitivity to external influences increases (Macotela et al., 2017; Raulin et al., 2014) allowing a wider range of physical and chemical processes to modify VLF propagation conditions. On the other hand, the size of SPP shown in Figure 5a varies from 5° to 50°. Although the observed SPP values show high correlation with ozone number density at ~40 km using 10-day averages, the large day-to-day variability observed, especially during wintertime, requires further study. In particular, preliminary additional correlation analysis between the ozone number density and the size of SPP variabilities, using averaging times shorter than five days, indicates good correlations as well as interesting differences that motivate us to address this further in future work. But in general, on a day-to-day basis the SPP size could be due to equivalent changes in ozone altitude distributions at ~40 km as suggested by Figure 4, or by negative ion chemistry in the *D* region.

5. Conclusions

In this paper we have investigated the physical causes of VLF sunrise phase perturbation variations observed during the sunrise transition period. VLF subionospheric radio wave signals from a UK transmitter, GVT, received in Sodankylä, Finland, were analyzed to determine the characteristics of sunrise phase recoveries over a seven-year period (2010–2017). The results of our study are the following:

1. The timing at the maximum of the sunrise phase perturbation has an annual pattern that is well described by the seasonal variation of the sunrise times at an altitude of 28 km above the VLF transmitter.
2. Atmospheric temperature variations in the altitude range 36–40 km are better correlated with the size of the sunrise phase perturbation than for temperatures at other altitudes.

3. Variations in ozone number density at 38–42-km altitudes are better correlated with the size of the sunrise phase perturbation than for ozone at other altitudes, and the analysis with ozone exhibits higher correlation with the VLF phase signal than atmospheric temperature.
4. Sunrise phase perturbations are generated by stratospheric ozone, as a result of UV shadowing on the ionospheric *D* region, generated by the absorption of solar UV flux having to pass through stratospheric ozone.

This work shows that various characteristics of VLF sunrise phase perturbation observed during sunrise transitions are caused by stratospheric ozone shadowing. The absorption of solar UV flux when the Sun is close to the horizon affects the formation of mesospheric electron number density profiles. This conclusion appears valid for multiday smoothed data, although day-to-day variability in the observed size of the sunrise phase perturbation values is larger than for ozone. This could be due to some of the previously considered sunrise phase perturbation mechanisms, such as negative ion chemistry.

Data Availability Statement

Data availability is described at the following websites: http://www.sgo.fi/Data/VLF/VLF.php (AARDDVARK) and https://mls.jpl.nasa.gov/products/temp_product.php (EOS MLS).

Acknowledgments
ELM was supported by the Suomen Kulttuurirahasto (grant 00180689) and the Oulun yliopiston tukisäätiö (grant 20180003). D.A.N. and M.A.C. were supported in part by the UK Natural Environment Research Council (grants NE/J022187/1 and NE/R016038/1).

References

Abdu, M. A., Ananthakrishnan, S., Krishnan, B. A., & Massambani, O. (1973). Cosmic ray ionization in the *D* region at sunrise: Evidence from VLF phase measurements. *Radio Science*, *8*(8–9), 733–736. https://doi.org/10.1029/RS008i008p00733

Bertoni, F. C. P., Raulin, J. P., Gavilán, H. R., Kaufmann, P., Rodriguez, R., Clilverd, M., et al. (2013). Lower ionosphere monitoring by the South America VLF Network (SAVNET): *C* region occurrence and atmospheric temperature variability. *Journal of Geophysical Research: Space Physics*, *118*, 6686–6693. https://doi.org/10.1002/jgra.50559

Bracewell, R. N., & Bain, W. C. (1952). An explanation of radio propagation at 16 kc/s in terms of two layers below *E* layer. *Journal of Atmospheric and Terrestrial Physics*, *2*(4), 216–225. https://doi.org/10.1016/0021-9169(52)90032-9

Bracewell, R. N., & Straker, T. W. (1949). The study of solar flares by means of very long radio waves. *Monthly Notices of the Royal Astronomical Society*, *109*, 28–45. https://doi.org/10.1093/mnras/109.1.28

Clilverd, M. A., Rodger, C. J., Thomson, N. R., Brundell, J. B., Ulich, T., Lichtenberger, J., et al. (2009). Remote sensing space weather events: Antarctic-Arctic Radiation-belt (Dynamic) Deposition-VLF Atmospheric Research Konsortium network. *Space Weather*, *7*, S04001. https://doi.org/10.1029/2008SW000412

Comarmond, J. M. (1977). Contribution a l'étude de la basse ionosphère par des mesures de phase et d'amplitude d'ondes électromagnétiques a très basse fréquence (Doctoral disserttion). Université Pierre et Marie Curie.

Hargreaves, J. K. (1962). The behaviour of the lower ionosphere near sunrise. *Journal of Atmospheric and Terrestrial Physics*, *24*(1), 1–7. https://doi.org/10.1016/0021-9169(62)90289-1

Hultqvist, B. (1966). Negative ions in the lowest ionosphere with special reference to experimental evidence from upper atmosphere research. *Annales de Geophysique*, *22*, 235–246.

Krasnushkin, P. E. (1962). On the propagation of long and very long radio waves around the Earth. *Supplemeto Nuovo Cimento*, *26*(1), 50–112. https://doi.org/10.1007/BF02782993

Kuntz, V. L. R., Piazza, L. R., & Kaufmann, P. (1991). *C*-layer dependence on solar cycle and southern latitude observed by VLF propagation. *Journal of Atmospheric and Terrestrial Physics*, *53*(5), 419–423. https://doi.org/10.1016/0021-9169(91)90036-7

Livesey, N., Read, W., Wagner, P., Froidevaux, L., Lambert, A., Manney, G., et al. (2017). *Version 4.2x Level 2 Data Quality and Description Document, Version 4.2x-3.1.* . Pasadena, CA: Jet Propulsion Laboratory. Retrieved from. https://mls.jpl.nasa.gov/data/v4-2_data_quality_document.pdf

Lynn, K. J. W. (2010). VLF waveguide propagation: The basics. *AIP Conference Proceedings*, *1286*(1), 3–41. https://doi.org/10.1063/1.3512893

Macotela, E. L., Raulin, J.-P., Manninen, J., Correia, E., Turunen, T., & Magalhães, A. (2017). Lower ionosphere sensitivity to solar X-ray flares over a complete solar cycle evaluated from VLF signal measurements. *Journal of Geophysical Research: Space Physics*, *122*, 12,370–12,377. https://doi.org/10.1002/2017JA024493

McRae, W. M., & Thomson, N. R. (2000). VLF phase and amplitude: Daytime ionospheric parameters. *Journal of Atmospheric and Solar-Terrestrial Physics*, *62*, 609–618. https://doi.org/10.1016/S1364-6826(00)00027-4

Mechtly, E. A. E., Bowhill, S. A., Smith, L. G., & Knoebel, H. W. (1967). Lower ionosphere electron concentration and collision frequency from rocket measurements of Faraday rotation, differential absorption, and probe current. *Journal of Geophysical Research*, *72*, 5239–5245. https://doi.org/10.1029/JZ072i021p05239

Mechtly, E. A. E., & Smith, L. G. (1968). Growth of the *D*-region at sunrise. *Journal of Atmospheric and Terrestrial Physics*, *30*, 363–369. https://doi.org/10.1016/0021-9169(68)90072-X

Moler, W. F. (1960). VLF propagation effects of a *D*-region layer produced by cosmic rays. *Journal of Geophysical Research*, *65*(5), 1459–1468. https://doi.org/10.1029/JZ065i005p01459

Nicolet, M., & Aikin, A. C. (1960). The formation of the D region of the ionosphere. *Journal of Geophysical Research*, *65*(5), 1469–1483. https://doi.org/10.1029/JZ065i005p01469

Ratcliffe, J. A. (1972). *An Introduction to the Ionosphere and Magnetosphere*. London: Cambridge University Press.

Raulin, J.-P., Trottet, G., Giménez de Castro, C. G., Correia, E., & Macotela, E. L. (2014). Nighttime sensitivity of ionospheric VLF measurements to X-ray bursts from a remote cosmic source. *Journal of Geophysical Research: Space Physics*, *119*, 4758–4766. https://doi.org/10.1002/2013JA019670

Reder, F. H., & Westerlund, S. (1970). VLF phase instabilities produced by propagation medium: Experimental results. In K. Davies (Ed.), *Phase and Frequency Instabilities in Electromagnetic Wave Propagation, AGARD Conference Proceedings* (Vol. 33, pp. 103–106). Boulder, CO: Environmental Science Services Administration.

Schaal, R. E., & Ananthakrishnan, S. (1970). Ozone screening heights deduced from sunrise effects at very low frequencies. *Journal of Atmospheric and Terrestrial Physics*, *32*, 1831–1834. https://doi.org/10.1016/0021-9169(70)90140-6

Sechrist, C. F. Jr. (1968). Interpretation of pre-sunrise electron densities and negative ions in the *D*-region. *Journal of Atmospheric and Terrestrial Physics*, *30*, 371–338. https://doi.org/10.1016/0021-9169(68)90109-8

Thomson, N. R., Clilverd, M. A., & Rodger, C. J. (2017). Midlatitude ionospheric *D* region: Height, sharpness, and solar zenith angle. *Journal of Geophysical Research: Space Physics*, *122*, 8933–8946. https://doi.org/10.1002/2017JA024455

Turco, R. P., & Sechrist, C. F. Jr. (1972). An investigation of the ionospheric *D* region at Sunrise: 3, time variations of negative-ion and electron densities. *Radio Science*, *7*(7), 725–737. https://doi.org/10.1029/RS007i007p00725

Wait, J.R., & Spies, K.P. (1964). Characteristics of the Earth-ionosphere waveguide for VLF radio waves. Volume NBS Technical Note 300 NIST Research Library.

Waters, J. W., Froidevaux, L., Harwood, R. S., Jarnot, R. F., Pickett, H. M., Read, W. G., et al. (2006). The Earth observing system microwave limb sounder (EOS MLS) on the aura satellite. *IEEE Transactions on Geoscience and Remote Sensing*, *44*(5), 1075–1092. https://doi.org/10.1109/TGRS.2006.873771